Nanosecond Time-Resolved Fluorescence Spectroscopy in the Physical Chemistry Laboratory: Formation of the Pyrene Excimer in Solution

David A. Van Dyke,* Brian A. Pryor, Philip G. Smith, and Michael R. Topp*
Department of Chemistry, University of Pennsylvania, Philadelphia, PA 19104-6323

Laser-based spectroscopic techniques have become firmly established in modern physical chemistry research because they are powerful tools for the study of atomic and molecular structure and dynamics. For example, a 1992 survey of experimental articles in issues of the *Journal of Physical Chemistry* and the *Journal of Chemical Physics* found that some 40% used lasers in some way (*1*). Until recently, however, very few undergraduate physical chemistry laboratories have incorporated laser spectroscopy experiments, so that few undergraduate students were exposed to this exciting and very important area of chemistry. This is reflected by the dearth of laser experiments in the chemical education literature prior to the present decade. (For a list of the experiments published before 1989, see the review by Steehler [*2*]). Progress in resolving this problem has appeared in the last few years with the publication of a number of new laser experiments for the physical chemistry laboratory, including no fewer than eight articles in a text devoted to modernizing the physical chemistry curriculum (*3*). A growing number of experiments are appearing in this *Journal* (*4–12*); other experiments were published in a book by Zare et al. (*13*) or are available from laser manufacturers (*14*). Many of these make use of moderately priced nitrogen/dye laser systems. These versatile devices have many potential applications in an undergraduate teaching laboratory, including moderately high-resolution spectroscopy via the use of associated dye lasers, and experiments employing nanosecond time resolution.

The experiment that we will describe here combines a nitrogen laser with a $^1/_4$-meter monochromator, a digital oscilloscope, and a computer-interfaced boxcar-gated integrator for nanosecond time-resolved fluorescence spectroscopy. The effective time resolution is <15 ns. Admittedly, more rigorous techniques such as time-correlated single-photon counting offer better time resolution (0.02–0.5 ns) and superior dynamic range, and thus are better suited for examining subtle changes in fluorescence time profiles. The lower precision of the nitrogen-laser techniques described here does limit the interpretation of the data to an extent. From a pedagogical standpoint, however, these laser experiments have the important advantage that the same instrumentation is used both to obtain emission spectra and to examine their time evolution, so that students can readily appreciate the complementary aspects of the spectral and kinetic data.

The experiment studies the excited-state behavior of pyrene (Fig. 1). The pyrene molecule offers two advantages: it absorbs strongly at the wavelength of the nitrogen laser, and it has a fairly long excited-state lifetime (e.g., 382 ns in deoxygenated cyclohexane [*15*]). In this experiment, several aspects of the fluorescence behavior of pyrene are studied, as follows.

1. The fluorescence emission spectra of solutions having different concentrations demonstrate the increasing formation of the excimer as the pyrene concentration is increased.
2. The fluorescence decay time profiles, monitored at various concentrations and several wavelengths, allow the lifetimes of the electronically excited primary and photoproduct species to be calculated.
3. The rate of excimer formation at higher concentrations depends on the solvent, and can be followed as a function of viscosity.
4. Dissolved oxygen reacts with the excited pyrene molecule at a rate close to that of molecular diffusion through solution, so that the fluorescence lifetime in dilute aerated solution also reflects solvent viscosity. Argon purging is shown to be an effective means to remove dissolved oxygen.

Others have previously published instructional experiments on the thermodynamics and kinetics of the formation of the pyrene excimer (*6, 16*). However, rather than simply focusing on the formation of the pyrene excimer, this experiment also uses the fluorescence of the pyrene molecule as a probe of solution-phase phenomena to illustrate such important concepts as diffusion-control of rates, quenching, and viscosity. The acquisition of emission spectra provides a qualitative illustration of the meaning of the kinetic data. And, very importantly, students gain hands-on experience with modern laser and spectroscopy equipment. They collect and analyze both spectral and kinetics data, and they also gain experience in computer-aided data acquisition and manipulation. To that end, we have attempted to maximize student control of the experiment, while taking advantage of the speed and graphics capability of desktop computers.

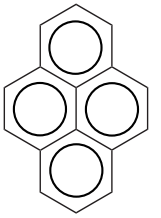

Pyrene

Figure 1. Molecular structure of pyrene.

Theoretical Background

When solutions of pyrene are irradiated by ultraviolet light, they produce fluorescence according to the scheme:

$$S_0 + h\nu_1 \rightarrow S^* \qquad \text{excitation} \qquad (1)$$

where S* = S_1, S_2, etc.

$$S_2 \rightarrow S_1\ (10^{-11}\ \text{s}) \qquad \text{internal conversion and vibrational cooling} \qquad (2)$$

$$S_1 \rightarrow S_0 + h\nu_2\ (4 \times 10^{-7}\ \text{s}) \qquad \text{fluorescence} \qquad (3)$$

*Corresponding authors. Current address for David Van Dyke: Department of Chemistry, Grand Valley State University, Allendale, MI 49401.

The long excited-state lifetime of pyrene provides a convenient window to observe fluorescence lifetime reduction with nanosecond-resolution equipment. However, since the fluorescence lifetime and the absorption strength are inversely related (*17*), small $S_0 \rightarrow S_1$ absorption cross sections potentially complicate experiments in dilute solutions. Fortunately, pyrene also has nearby a strong $S_0 \rightarrow S_2$ absorption transition. Figure 2 shows the absorption spectrum of pyrene in hexane, revealing the great difference in absorption strengths of the $S_0 \rightarrow S_1$ and $S_0 \rightarrow S_2$ transitions. The intense $S_0 \rightarrow S_2$ band has a maximum at ≈335 nm, which is close to the nitrogen laser wavelength of 337.1 nm. On the other hand, the $S_0 \rightarrow S_1$ transitions are only revealed at high sensitivity as weak transitions on the long-wavelength edge of this spectrum. In fluid solutions, the excitation energy does not affect the present experiments (Kasha's rule), since the excess energy over the S_1 state is dissipated by solute–solvent collisional energy transfer on a time scale of ≤ 50 ps, much less than the fluorescence lifetime. Therefore, it is possible to excite the molecule via the strong $S_0 \rightarrow S_2$ transition and yet study the longer-lived S_1 state. (As an aside, Figure 2 shows that pyrene absorbs significantly at both 355 and 266 nm, which correspond to the third and fourth harmonics, respectively, of an Nd:YAG laser. Because modestly priced, easily installed Nd:YAG lasers are now commercially available, it is important to note that an Nd:YAG laser is also a feasible source for carrying out the experiments described below.)

Several other relaxation processes remove the excited S_1 state and effectively shorten the fluorescence lifetime, including intersystem crossing to the triplet state and quenching:

$$S_1 \rightarrow T_1 \qquad \text{intersystem crossing} \qquad (4)$$

$$S_1 + Q \rightarrow S_0 + Q^* \qquad \text{quenching by energy transfer} \qquad (5)$$

Relaxation to the triplet excited state via intersystem crossing is usually a significant process for aromatic molecules following population of the S_1 state; the intersystem crossing efficiency for pyrene is about 38% in ethanol (*18*). A universally important bimolecular quenching process involves molecular oxygen, which is paramagnetic by virtue of its triplet ground state. It is an excellent quencher of both singlet and triplet electronically excited molecules. Although the process by which oxygen quenches the S_1 state of aromatic hydrocarbons is complex (*19, 20*), the net reaction in low-viscosity solution involves low-lying singlet states of oxygen (*21*):

$$S_1 + O_2\,(^3\Sigma_g^-) \rightarrow T_1 + O_2\,(^1\Sigma_g^+, {}^1\Delta_g) \qquad (6)$$

Aromatic molecules in the S_1 state can also undergo a number of other photochemical processes. One common process is the reaction of the excited singlet with a ground state molecule of the same type, yielding an electronically excited dimer known as an *excimer*:

$$S_1 + S_0 \rightarrow \{S_0S_1\} \qquad \text{excimer formation} \qquad (7)$$

The pyrene excimer was the first species of this type to be discovered (*22–25*). The fluorescence of the excited monomer is violet, with λ_{max} = 377 nm, and the spectrum has considerable structure due to transitions to different vibrational levels of the ground state. The presence of this structure shows that both the molecular ground and excited states are stable but differ slightly in structure. Also, the nearby S_2 state "promotes" the $S_0 \rightarrow S_1$ transition. However, the blue fluorescence from

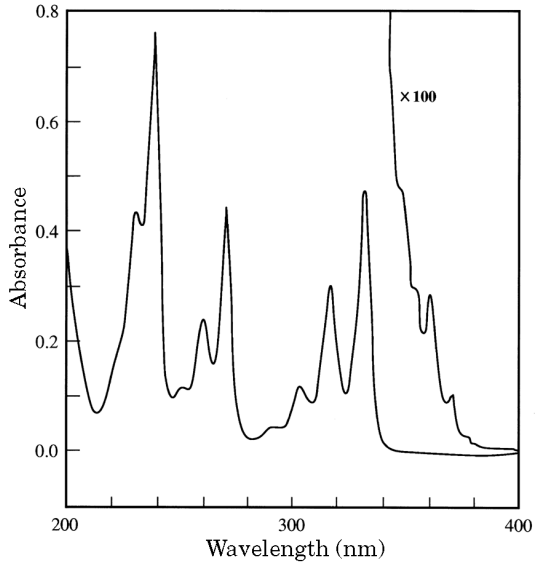

Figure 2. Absorption spectrum of 1.0×10^{-5} M pyrene in hexane, 1 mm cell, showing the $S_0 \rightarrow S_1$ and $S_0 \rightarrow S_2$ regions.

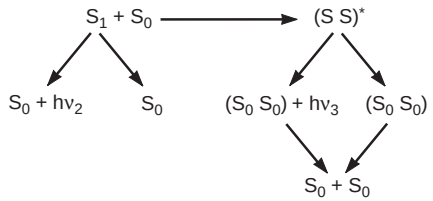

Figure 3. Proposed reaction scheme for pyrene photophysics in solution (*23*).

the excimer, with λ_{max} = 480 nm, exhibits a broad structureless band, reflecting the fact that the double molecule does not have a bound ground state. Thus, it rapidly dissociates into two ground-state monomers following fluorescence emission.

Förster and Kasper (*22, 23*) first deduced the existence of the excimer from the progressive disappearance of emission at 377 nm and the growth of emission at 480 nm as pyrene concentration was increased, even though the concentration changes did not affect the shape of the absorption spectrum. They proposed the mechanism shown in Figure 3. The rate expressions for their scheme are:

$S_0 + h\nu_1 \rightarrow S_1$	Rate = I_{abs}	excitation	(8)
$S_1 \rightarrow S_0 + h\nu_2$	$k_f[S_1]$	fluorescence	(9)
$S_1 \rightarrow\!\!\rightarrow S_0$	$k_n[S_1]$	nonradiative de-excitation	(10)
$S_1 \rightarrow T_1$	$k_g[S_1]$	intersystem crossing	(11)
$S_1 + S_0 \rightarrow\!\!\rightarrow \{SS\}^*$	$k_A[S_1][S_0]$	excimer formation	(12)
$\{SS\}^* \rightarrow\!\!\rightarrow S_1 + S_0$	$k_d[\{SS\}^*]$	excimer dissociation	(13)
$\{SS\}^* \rightarrow S_0 + S_0 + h\nu_3$	$k'_f[\{SS\}^*]$	excimer fluorescence	(14)
$\{SS\}^* \rightarrow\!\!\rightarrow S_0 + S_0$	$k'_n[\{SS\}^*]$	excimer nonradiative de-excitation	(15)

The experiments described here allow students to understand the role of a fluorescent probe in examining elements of such a reaction scheme.

Experimental Procedure

CAUTION: A number of potential hazards are associated with the use of nitrogen lasers, including powerful pulses of invisible ultraviolet radiation capable of permanently damaging eyesight and burning skin, lethal voltages present inside the laser, ozone generation, and the use of high-pressure compressed gas cylinders. The laser should be set up so that the beam is kept below eye level and always contained within beam guides and a sample compartment with nonreflective surfaces. Laboratory safety glasses (with side shields) must be worn at all times to protect against incidental laser exposure and chemical hazards. Because nitrogen lasers can generate significant levels of ozone, the experiment must be carried out in a well-ventilated room, preferably with a ventilation manifold just above the laser.

This experiment was carried out with the apparatus diagrammed in Figure 4. The nitrogen laser used was a Laser Photonics LN1000, which produces 1.4-mJ pulses of ≈ 600 ps duration at 337.1 nm, at repetition rates of up to 20 Hz. Such short pulses ensure that the experimental time resolution is limited only by the detection electronics. The laser output is aligned with the front corner of the sample cuvettes to reduce inner filter effects on the shapes of the emission spectra. Disposable methacrylate cuvettes (Fisher Scientific) were found to yield adequate results. The fluorescence output was measured at 90° to the incident beam direction by focusing the fluorescence onto the entrance slit of a $^1/_4$-m monochromator (PTI Model 001). The amount of fluorescence passing into the monochromator could be controlled by neutral density filters in front of the entrance slit. An R928 or 1P21 photomultiplier tube (PMT) in a Model PR-1405RF housing (Products for Research) was mounted at the output of the monochromator. The monochromator was tuned via a digital stepper motor controller. The output from the PMT, which was powered by a stabilized dc power supply, was fed into a Stanford Research Systems Model 250 boxcar-gated integrator. The hardware incorporated an SR280 mainframe, SR245 computer interface, and SR270 data acquisition program run on a personal computer. The data were fitted to up to three exponentials via a simple algorithm written within the Sigma Plot graphics program:

$$I(t) = \sum_i c_i e^{-k_i(t)} \qquad (16)$$

The fast instrument response could be treated as a delta function with little error in most experiments. Otherwise, a finite instrument-function width could be formally deconvoluted from the data.

Nitrogen lasers often have timing jitter between the trigger pulse and the optical output on the order of 10–20 ns. One needs to eliminate this source of jitter to provide a more representative measurement of the instrument response function. In this experiment, we triggered the boxcar by allowing residual laser radiation to fall onto a fluorescent target, which in turn activated a fast PIN diode detector (Thor Labs #DE2-SL). The diode output was fed directly into the trigger of the boxcar integrator. Also, to allow for the throughput delay of the electronics, the PMT output signal was delayed by passing through a 12.2-m coaxial cable (≈60 ns transit time). In this way, the boxcar could scan baseline signal before the arrival of the laser pulse. The instrument response function recorded

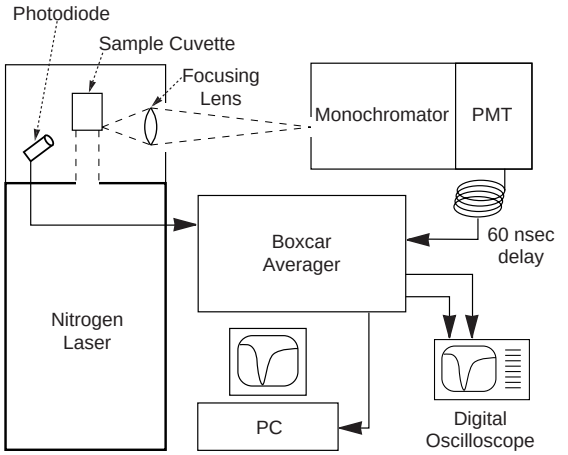

Figure 4. Laser apparatus for nanosecond transient spectroscopy.

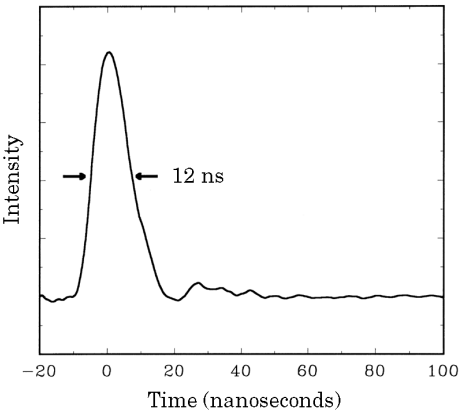

Figure 5. Representative instrument response profile measured using scattered laser radiation.

from scattered laser radiation is shown in Figure 5; the full width at half-maximum intensity was about 12 ns.

The PMT signal was simultaneously displayed on a Tektronix Model 2232 100-MHz digital storage oscilloscope, which was triggered by the BUSY output from the boxcar. This arrangement enabled both the laser pulse and the fluorescence decay profiles to be viewed on the oscilloscope, allowing students to appreciate more readily the events being recorded by the boxcar integrator. This is particularly useful when recording emission spectra. As a precautionary note, one needs to use calibrated neutral density filters to establish the signal range over which the photomultiplier response is linear. This procedure is required for fitting kinetic models to the experimental data. For the present experiments, *n*-hexane and *n*-tetradecane (chromatographic grade) were chosen as solvents for pyrene because their viscosity coefficients differ by a factor of ≈ 7: η(hexane) = 0.300 cP and η(tetradecane) = 2.128 cP, both measured at 25 °C (*26*). This choice gives a useful range of resolvable solvent–viscosity effects. Pyrene was obtained from Aldrich and used as received.

CAUTION: Gloves should be worn when handling pyrene. Thorough washing with soap and water is necessary in case of skin contact with pyrene solid or solutions. *n*-Hexane is very volatile and flammable. Hexane solutions must be kept away from open flames and electrical equipment.

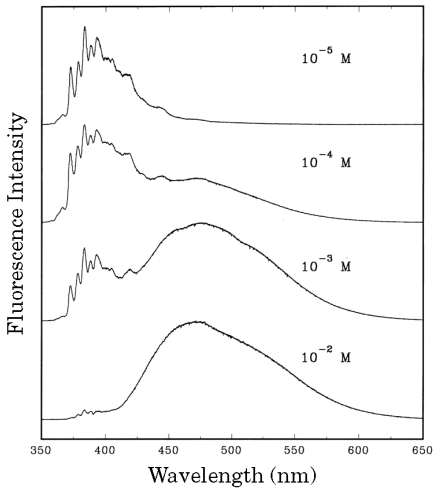

Figure 6. Pyrene emission spectra as a function of concentration: 10^{-2} to 10^{-5} M in hexane.

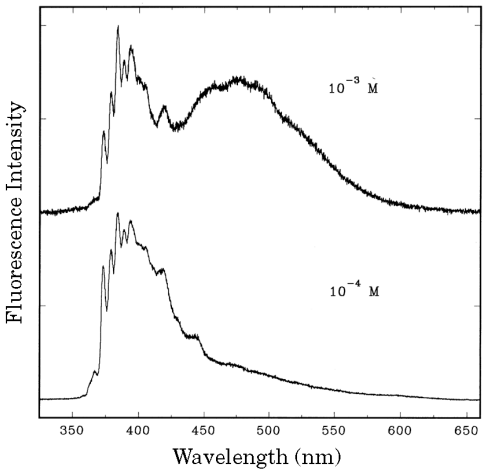

Figure 7. Pyrene emission spectra as a function of concentration: 10^{-3} and 10^{-4} M in tetradecane.

Solutions were deoxygenated by capping the cuvette with aluminum foil and gently bubbling argon into the solution through a Teflon capillary tube. Argon purging was continued for the duration of a run to ensure that the oxygen concentration remained low. [NOTE: An alternative procedure to remove oxygen, which is more involved but more effective, involves freeze–pump–thaw preparation of solutions in vacuum-sealed cuvettes. This was not used in the experiments reported here.]

Results

Emission Spectra

Emission spectra were recorded by fixing the delay of the boxcar gate and scanning the wavelength of the monochromator. Figure 6 compares several spectra for pyrene concentrations of 10^{-2}–10^{-5} M in deoxygenated *n*-hexane, observed via a long gate setting on the boxcar. A sampling gate width $\geq$500 ns ensures that all temporal components of the fluorescence are collected, so that the resulting spectra are similar to those that would be recorded on a spectrofluorimeter. The spectra in Figure 6 show the evolution from mostly short-wavelength (monomer) emission at low concentration to mostly long-wavelength (excimer) emission at high concentrations.

Students can also usefully compare the fluorescence spectra of pyrene solutions in tetradecane. At concentrations $\leq 10^{-5}$ M, the emission spectra in the two solvents are nearly the same because there is little excimer formation. However, the experimental results in Figure 7 clearly show that for 10^{-4} and 10^{-3} M concentrations of pyrene in tetradecane, the excimer/monomer ratio is appreciably less than in the corresponding hexane solutions. This comparison therefore shows that the average fluorescent species in pyrene solutions depends on both concentration and solvent viscosity. The lower viscosity of the hexane solution allows the solute molecules to diffuse more rapidly through solution, promoting the excimer formation reaction.

Gated Emission Spectra

Reducing the boxcar gate width allows one to observe the time sequence of fluorescent events. In this way, one may *directly* examine the *temporal* properties of the spectral components (*27*). Thus, Figure 8 shows four gated emission spectra (gate width = 2 ns) taken at different times after the laser pulse, for a solution of 5×10^{-3} M pyrene in argon-purged *n*-tetradecane. Here, the spectrum taken at "zero" time (i.e., coinciding with the laser pulse) shows nearly pure monomer emission. At longer times, students can observe that excimer emission becomes the dominant component. One may note also that the zero-time spectra contain scattered light signals from the exciting nitrogen laser, which can be used to calibrate the spectrum. These "goal posts" arise from first- and second-order reflections of the grating in the detection monochromator, at 337.1 nm and 2×337.1 nm, respectively.

Fluorescence Time Profiles: Excimer Formation and Decay

If instead of scanning wavelength at fixed gate time, if time is scanned at a fixed wavelength, then traces such as those in Figure 9 are obtained.[1] This figure, recorded under almost the same conditions as Figure 8, shows complementary traces monitored at 380 nm (i.e., monomer) and 480 nm (i.e., excimer). The time profile at 380 nm fits a first-order decay profile:

$$I(t) = A_0 e^{-k_a t} \qquad (17)$$

where k_a = 0.0056 ns^{-1}, corresponding to a decay time of 180 ns. Also noting that the fluorescence decay time of the monomer in argon-purged tetradecane is $\approx$400 ns ($k \approx 0.0025$ ns^{-1}), we can calculate the pseudo-first-order nonradiative rate constant for excimer formation to be ≈ 0.0031 ns^{-1}. Given the concentration of 1.0×10^{-3} M, this gives the second-order rate constant as 3.0×10^{9} $M^{-1}s^{-1}$.

The complementary trace for the excimer fluorescence, showing a fast rise time and slower fall time, is compared against a fitted curve in Figure 9. The fit was according to

$$I(t) = -Ae^{-k_a t} + Be^{-k_b t} \qquad (18)$$

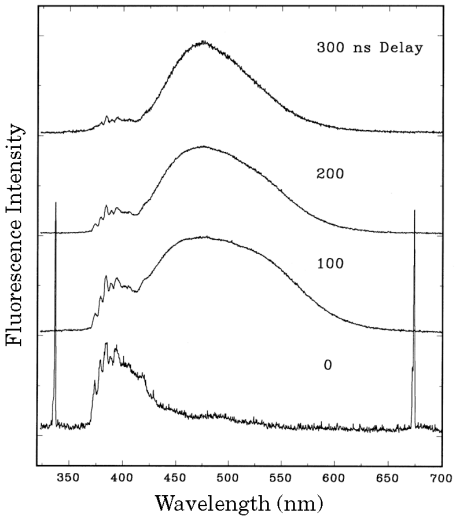

Figure 8. Emission spectra for pyrene (5×10^{-3} M) in tetradecane, obtained at different gate times after excitation.

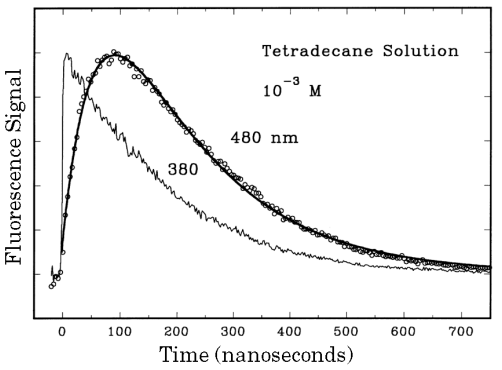

Figure 9. Time scans of 10^{-3} M pyrene solution in tetradecane, showing evolution of the spectrum paralleling the data of Figure 8. "380" represents the monomer time profile. Circles represent the experimental data for the excimer, monitored at 480 nm. Solid line is a double-exponential fit (see text).

where k_a = 0.0058 ns^{-1} and k_b = 0.0173 ns^{-1}. The value of k_a obtained from both traces is consistent. Also, the value of k_b represents a fluorescence decay time for the excimer of 58 ns. On closer inspection, the form of the 480 nm curve in Figure 9 appears counterintuitive, since the fast rise time of the excimer fluorescence is faster than the decay time for the monomer. To explain this, consider that the concentration of an intermediate species B in a consecutive first-order reaction sequence has a time dependence according to

$$I(t) = A_0\left(\frac{k_a}{k_b - k_a}\right)\left(e^{-k_a t} - e^{-k_b t}\right) \qquad (19)$$

Here, the constant A_0 is, of course, positive. On the one hand, if $k_a >> k_b$ (i.e., B is a long-lived product), the leading edge of the profile would be determined by the relaxation dynamics of species A. However, if $k_a << k_b$ (i.e., the case of a short-lived product), because of the change in sign of the denominator, the leading edge will more closely resemble the relaxation dynamics of species B. In the present experiment, since the excimer (B) has an intrinsically shorter fluorescence decay time than the monomer (A), the second case applies. Therefore, the relatively fast rise time of the excimer seen in Figure 9, as compared with the decay of the monomer, actually corresponds to the decay time profile of the excimer.

It is also instructive to compare the calculated second-order rate constant with predictions from the Debye equation:

$$k_q = \frac{8000\,RT}{3\eta}\ \text{L mol}^{-1}\text{s}^{-1} \qquad (20)$$

where the quantity η is expressed in the units of N m^{-2} s (≡ Pa s). The value of η for tetradecane is 2.128 cP (= 2.128×10^{-3} N m^{-2} s), giving rise to $k_q \approx 3.10\times10^9$ M^{-1} s^{-1}. This value is in reasonable agreement with the experimental measurement, especially considering our assumption of a molecular solution (i.e., this approach assumes that molecules diffuse from infinity through a solvent of pure tetradecane).

Fluorescence Time Profiles: Oxygen Quenching

In another aspect of the experiment, one may quantitatively analyze the effect of oxygen on the fluorescence lifetime. Thus, the fluorescence time-profile is measured for 10^{-5} M pyrene in *n*-hexane. In this concentration regime, we can be sure that the solute minimally perturbs the solvent and that solute–solute interactions are negligible on the time scale of the fluorescence lifetime. The monomer lifetime in the argon-purged solution is ≈ 400 ns ($k = 2.5\times10^6$ s^{-1}), whereas in air-saturated solution it is ≈ 14 ± 3 ns ($k \approx 7.1\times10^7$ s^{-1}). The difference, amounting to $\approx 6.9\times10^7$ s^{-1}, can be equated to $k_q[O_2]$, which is the pseudo-first-order rate constant for quenching of the singlet. Thus, according to the scheme of Figure 3, we may add another term to the first-order kinetics of S_1 pyrene:

$$k_{Total} = k_f + k_n + k_g + k_q[O_2] + k_A[S_0] \qquad (21)$$

where the first three terms account for the 400-ns lifetime in the absence of O_2. At 10^{-5} M concentration, the spectrum shows little evidence of excimer formation, which suggests that the last term can be neglected.

We can again use the Debye equation for comparison, this time for estimating the concentration of oxygen in solution. The value of η for hexane is 0.300 cP (= 3.00×10^{-4} N m^{-2} s), giving rise to $k_q \approx 2.2\times10^{10}$ $M^{-1}s^{-1}$. From this we calculate the concentration of oxygen in solution to be

$$[O_2] = (6.9\times10^7\ s^{-1})/(2.2\times10^{10}\ \text{L mol}^{-1}\ s^{-1}) = 3.1(\pm0.7)\times10^{-3}\ \text{M} \qquad (22)$$

This is consistent with literature values for the concentration of oxygen in air-saturated hexane, 3×10^{-3} M (*28*).

Conclusion

In the junior-level experimental physical chemistry class at the University of Pennsylvania, this sequence of experiments is performed by teams of two students over the course of four 4-hour laboratory periods. During the first lab period, the students prepare their solutions and begin learning

how to operate the instruments by observing as the preceding group finishes their data collection. During the second and third lab periods, the students collect the spectral and time profile data. The fourth lab period is spent in analyzing the data on a separate computer. Thus, a new team of students can begin the experiment every second lab period. Through this sequence of experiments, they are introduced to several different aspects of fluorescence spectroscopy and kinetic analysis. They also get hands-on experience with a pulsed laser, nanosecond-synchronized detection electronics, and computer-aided data analysis. The experimental preparations are very straightforward, and students can acquire a good working knowledge of the experimental procedures in a single afternoon. The quality of the fluorescence time profiles is not as good as that obtainable from a photon-counting experiment, especially in signal-to-noise ratio and time resolution. On the other hand, the present experiment is relatively inexpensive to run and has the advantage that students can obtain both spectroscopic and kinetic information on the same apparatus. Finally, one should note that the experiment is very flexible, and could be applied to many other solvation interactions, such as excited-state proton or electron donor-acceptor reactions, with only minor changes in procedure.

Acknowledgments

We thank the National Science Foundation for an Instrumentation and Laboratory Improvement Program Grant (USE92-51664); and Laser Photonics, Inc., and Tektronix, Inc., for discounts and contributions, which made possible the purchase of the nitrogen laser system and the digital oscilloscope used in this work. Special credit must also go to the members of the Chemistry 223 (Experimental Physical Chemistry) course at the University of Pennsylvania who served as guinea pigs for the development of this experiment.

Note

1. Time-scan data can also be collected and averaged efficiently with a sufficiently fast digital oscilloscope interfaced to a computer with appropriate software for fitting exponentials. The use of the boxcar integrator here has the advantage of allowing students to collect and compare both wavelength-scan and time-scan data from a single solution in rapid succession without the need to reconfigure the experimental apparatus or leave the boxcar data acquisition software.

Literature Cited

1. Moore, R. J.; Schwenz, R. W. *J. Chem. Educ.* 1992, *69*, 1001–1002.
2. Steehler, J. K. *J. Chem. Educ.* 1990, *67*, A65–A71.
3. *Physical Chemistry: Developing a Dynamic Curriculum*; Schwenz, R. W.; Moore, R. J., Eds.; American Chemical Society: Washington, DC, 1993; Chapters 6–13.
4. Grant, C. A.; Hardwick, J. L. *J. Chem. Educ.* 1997, *74*, 318–321.
5. Muenter, J. S. *J. Chem. Educ.* 1996, *73*, 576–580.
6. Muenter, J. S.; Deutsch, J. L. *J. Chem. Educ.* 1996, *73*, 580–585.
7. DeGraff, B. A.; Horner, D. A. *J. Chem. Educ.* 1996, *73*, 279–285.
8. Hair, S. R. *J. Chem. Educ.* 1996, *73*, A7–A9.
9. O'Brien, L. C.; Kubicek, R. L. *J. Chem. Educ.* 1996, *73*, 86–87.
10. Fitzwater, D. A.; Thomasson, K. A.; Glinski, R. J. *J. Chem. Educ.* 1995, *72*, 187–189.
11. Galloway, D. B.; Ciolkowski, E. L.; Dallinger, R. F. *J. Chem. Educ.* 1992, *69*, 79–83.
12. King, M. E.; Pitha, R. W.; Sontum, S. F. *J. Chem. Educ.* 1989, *66*, 787–790.
13. Zare, R. N.; Spencer, B. H.; Springer, D.; Jacobson, M. *Laser Experiments for Beginners*; University Science Books: Mill Valley, CA, 1995.
14. For example, Ham, D.; Rigos, D. *Chemistry Experiments Using LSI Lasers for Physical Chemistry Laboratory Courses*; Laser Science, Inc.: Newton, MA, 1992.
15. Karpovich, D. S.; Blanchard, G. J. *J. Phys. Chem.* 1995, *99*, 3951–3958.
16. Halpern, A. M.; Reeves, J. H. *Experimental Physical Chemistry: A Laboratory Textbook*; Scott Foresman: Glenview, IL, 1988; pp 351–362.
17. Berlman, I. B. *Handbook of Fluorescence Spectra of Aromatic Molecules*, 2nd ed.; Academic: New York, 1971; pp 20–21, 383–385.
18. Horrocks, A. R.; Wilkinson, F. *Proc. R. Soc. London, Ser. A* 1968, *A306*, 257–273.
19. Birks, J. B. *Photophysics of Aromatic Molecules*; Wiley: New York, 1970; pp 492–502.
20. Birks, J. B. In *Organic Molecular Photophysics*; Birks, J. B., Ed.; Wiley: New York, 1975; Vol. 2, pp 545–549.
21. Calvert, J. G.; Pitts, J. N. *Photochemistry*; Wiley: New York, 1966; p 180.
22. Förster, Th.; Kasper, K. *Z. Phys. Chem.* 1954, *N.F.1*, 275–277.
23. Förster, Th.; Kasper, K. *Z. Elektrochem., Ber. Bunsen-Ges. Phys. Chem.* 1955, *59*, 976–980.
24. Birks, J. B.; Dyson, D. J.; Munro, I. H. *Proc. R. Soc. London* 1963, *A275*, 575–588.
25. Birks, J. B.; Lumb, M. D.; Munro, I. H. *Proc. R. Soc. London* 1964, *A280*, 289–297.
26. *Handbook of Chemistry and Physics*, 74th ed.; Lide, D. R.; Frederikse, H. P. R., Eds.; CRC: Boca Raton, FL, 1993; pp 6-196, 6-197.
27. Yoshihara, K.; Kasuya, T. *Chem. Phys. Lett.* 1971, *9*, 469–472.
28. *IUPAC Solubility Data Series: Oxygen and Ozone*; Battino, R., Ed.; Pergamon: Oxford, England, 1981; Vol. 7, pp 218–219, 235. *Handbook of Chemistry and Physics*, 74th ed.; Lide, D. R.; Frederikse, H. P. R., Eds.; CRC: Boca Raton, FL, 1993; pp 3-273, 14-12.